# Enhancement of Thermal Conductance at Metal-Dielectric Interfaces Using Subnanometer Metal Adhesion Layers

Minyoung Jeong,[1] Justin P. Freedman,[1] Hongliang Joe Liang,[2] Cheng-Ming Chow,[2] Vincent M. Sokalski,[1] James A. Bain,[2] and Jonathan A. Malen[1,3,*]

[1]*Department of Materials Science and Engineering, Carnegie Mellon University, Pittsburgh, Pennsylvania 15213, USA*

[2]*Department of Electrical and Computer Engineering, Carnegie Mellon University, Pittsburgh, Pennsylvania 15213, USA*

[3]*Department of Mechanical Engineering, Carnegie Mellon University, Pittsburgh, Pennsylvania 15213, USA*

(Received 4 September 2015; revised manuscript received 4 December 2015; published 26 January 2016)

We show that the use of subnanometer adhesion layers significantly enhances the thermal interface conductance at metal-dielectric interfaces. A metal-dielectric interface between Au and sapphire ($Al_2O_3$) is considered using Cu (low optical loss) and Cr (high optical loss) as adhesion layers. To enable high throughput measurements, each adhesion layer is deposited as a wedge such that a continuous range of thicknesses could be sampled. Our measurements of thermal interface conductance at the metal-$Al_2O_3$ interface made using frequency-domain thermoreflectance show that a 1-nm-thick adhesion layer of Cu or Cr is sufficient to enhance the thermal interface conductance by more than a factor of 2 or 4, respectively, relative to the pure $Au/Al_2O_3$ interface. The enhancement agrees with the diffuse-mismatch-model-based predictions of accumulated thermal conductance versus adhesion-layer thickness assuming that it contributes phonons with wavelengths less than its thickness, while those with longer wavelengths transmit directly from the Au.

DOI: 10.1103/PhysRevApplied.5.014009

## I. INTRODUCTION

Recent advances in modern microtechnologies and nanotechnologies have opened new possibilities for smaller, yet faster and more efficient electronic and optoelectronic devices. The optimal performance of these small devices requires effective thermal management, even at the level of interfaces due to the increased surface-to-volume ratio that accompanies reduced dimensions [1–4]. For example, heat-assisted magnetic recording (HAMR) is a promising option for the next generation of data storage in which interfacial thermal properties play a critical role. In this technology, a near-field transducer (NFT) heats the magnetic media in a localized region (~50 nm) through the delivery of electromagnetic radiation focused by a gold- (Au-)dielectric plasmonic interface [5–7]. Heat generated due to parasitic losses in the Au itself is dissipated to the dielectric and results in peak NFT temperatures that are hundreds of degrees above the ambient temperature [5]. High thermal-conductivity dielectrics such as aluminum nitride (AlN) or sapphire ($Al_2O_3$) would be preferred, therein making their interface with Au the clear bottleneck to heat dissipation.

The rate of heat transfer across the interface is described in terms of the thermal interface conductance ($G$), defined as $q''/\Delta T$, where $q''$ is the heat flux across an interface, and $\Delta T$ is the temperature difference across the interface [8]. The reported values of $G$ for the $Au/Al_2O_3$ interface range from 22 to 66 $MW\,m^{-2}\,K^{-1}$ at a temperature of 300 K [9,10], which is low compared to other metal-dielectric interfaces [10,11]. The Kapitza length, defined as $\kappa/G$, represents the thickness of a material with thermal conductivity $\kappa$ that has an equivalent resistance to the interface. Taking $\kappa$ of $Al_2O_3$ as 38 $W\,m^{-1}\,K^{-1}$ [12], and using the aforementioned $G$, the Kapitza length of $Al_2O_3$ ranges from 575 nm to 1.72 $\mu$m, which is far larger than typical NFT dimensions or the distance within the dielectric over which the temperature around the NFT drops [5].

Electrons are the main heat carriers in metals, while phonons are the main heat carriers in crystalline dielectrics. It has been proposed that electrons first transfer their energy to phonons in the metal with an equivalent conductance of $G_{e\text{-}p}$, and the phonons in the metal then transmit through the interface into the dielectric with $G_p$. Because these processes represent thermal resistances in series, $G$ becomes $(G_{e\text{-}p}G_p)/(G_{e\text{-}p}+G_p)$ [13–20]. The ratio of $G_{e\text{-}p}/G_p$ in the $Au/Al_2O_3$ interface is nearly 5 [13,21]. Because $G_{e\text{-}p}$ is larger, as shown by Wang *et al.* [22], the $G_p$ term becomes a bottleneck in the overall $G$. Notably, Wang *et al.* showed that temperature-dependent measurements of the electron-phonon coupling constant in thin films agree with Kagnov's classical theory for bulk

*jonmalen@andrew.cmu.edu

 

materials [22,23]. Thus, understanding and enhancing phonon transport across the interface is essential.

One possible approach to enhance $G$ is to insert adhesion layers between the two materials [24]. Good candidate materials should possess similar Debye temperatures to the substrate [10,11,25], with strong adhesion and affordable costs. For plasmonic technologies, the optical properties of an adhesion layer, which will impact the plasmonic properties of a Au-dielectric interface, are also critically important. Ideally, the adhesion-layer thickness would be minimized to maintain the plasmonic properties, but it is not precisely known how thick an adhesion layer is required to improve thermal performance.

In this study, we seek to answer how thick an adhesion layer is required to provide thermal benefits at a plasmonic interface. Frequency-domain thermoreflectance (FDTR), a noncontact optical technique, is used to experimentally measure $G$ across a $Au/Al_2O_3$ interface as a function of adhesion-layer thickness. In order to sample fine increments of thickness, the adhesion layers are deposited in a wedge shape on $Al_2O_3$ wafers such that a continuous taper from 0 to ∼7 nm exists. Cu and Cr adhesion layers are considered because they represent low- and high-optical loss metals in the near infrared (IR), yet both have higher Debye temperatures than Au. The experimentally measured $G$ values are then compared to diffuse-mismatch-model-(DMM-)based predictions to determine whether or not phonon alignment alone could account for observed enhancements of $G$ in adhesion layers that are just 1 nm thick.

## II. EXPERIMENT

Thin films are deposited on three-inch $Al_2O_3$ $c$-plane (0001) wafers by dc magnetron sputtering from five-inch targets in an argon atmosphere with a base pressure maintained at $< 2 \times 10^{-7}$ Torr. Substrates are cleaned with acetone in an ultrasonic bath for 10 min and then rinsed with isopropyl alcohol. Cr and Cu deposition rates are 0.67 Å $s^{-1}$ at 5 mTorr and 2.25 Å $s^{-1}$ at 2.5 mTorr, respectively.

Wedge films are prepared by moving the substrate into the target's deposition window at a controlled velocity before reversing the direction so that the leading edge is exposed to the plasma longer than the trailing edge. This process results in a thickness gradient with a targeted range between 0 and 6–8 nm. A 70-nm Au transducer layer of uniform thickness is deposited in a nonwedge shape on each of the adhesion layers without breaking the vacuum as shown in Fig. 1. Cu and Cr samples are fabricated additionally without Au for AFM analysis. AFM images taken at various positions on the wedge verify that the adhesion layers are deposited as continuous films without islanding. The spatially varying thickness of each adhesion layer and the Au layer are measured using x-ray reflectivity (XRR).

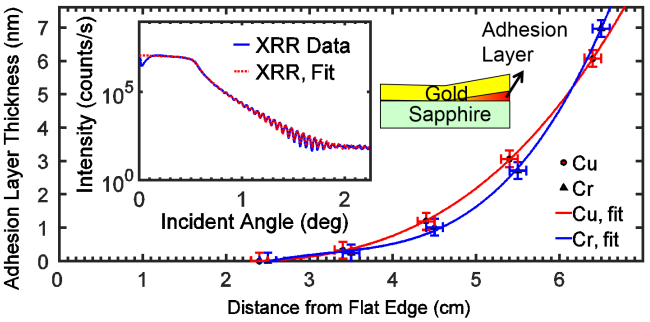


FIG. 1. Cu and Cr adhesion-layer thickness as a function of position on the substrate. Third-order polynomial fits for both experimental data are added. The inset schematic shows the adhesion-layer wedge. The inset plot shows XRR data and fits for a 1.20-nm-thick position on the Cu wedge.

The uncertainty in XRR data fitting of the adhesion-layer thickness is ±0.3 nm [26].

The thermal-interface-conductance values at the metal-$Al_2O_3$ interface are measured as a function of the adhesion-layer thickness by FDTR [27–29]. In this technique an electro-optic modulator intensity modulates a 488-nm continuous-wave pump laser over a range of frequencies (from 200 kHz to 10 MHz in this study). When the modulated pump beam is absorbed by the sample surface it periodically heats the sample at the pump-beam modulation frequency. This periodic heating generates corresponding changes in temperature at the surface that have a phase lag relative to the heating that depends on $G$. This periodic temperature response is detected by a 532-nm continuous-wave probe laser beam that is coaligned with the pump at the sample surface. The phase-lag data between the reflected pump and the probe beams at different positions on the substrate are obtained using a lock-in amplifier. A total of 40 data points are collected at each frequency and then fit to a widely used analytical solution of the heat diffusion equation [30]. By fitting this model to $G$ at each position on the wafer we extracted $G$ at different adhesion-layer thicknesses. The values and uncertainties in the fitting parameters are shown in Table I.

In modeling the system several parameters and assumptions are equivalently applied to all data points. The Au thermal conductivity ($k_{Au}$) for each sample is calculated using the Wiedmann-Franz law based on the electrical conductivity measured by a four-point probe on a region of the sample without the adhesion layer. The Au is modeled as isothermal, as Refs. [34,35], to mimic energy deposition at a finite depth and electron-phonon equilibration length scales of ∼100 nm [22]. To include this effect we reduced the Au thickness to 1 nm (from ∼$X$ nm), multiplied its heat capacity by $X$ so the total heat capacity is unchanged, and multiplied its Wiedmann-Franz thermal conductivity by $X$ so in-plane conduction is unchanged. The adhesion layer is modeled with the Au thermal conductivity. Since the adhesion layer is thinner than electron mean free paths,

TABLE I. Layer properties for FDTR analysis [31–33].

| Layer | Thickness (nm) | $k$ ($\mathrm{Wm^{-1}\,K^{-1}}$) | Heat Capacity ($\mathrm{Jkg^{-1}\,K^{-1}}$) | Density ($\mathrm{g/cm^3}$) |
|---|---|---|---|---|
| Au layer | $71 \pm 2.0$ (Cu sample)<br>$70 \pm 2.0$ (Cr sample) | $146 \pm 4.0$ (Cu sample)<br>$161 \pm 5.0$ (Cr sample) | $126 \pm 3.0$ | $19.3 \pm 0.4$ |
| Cu layer | Fig. 1 | $146 \pm 4.0$ | $390 \pm 5.0$ | $9.0 \pm 0.2$ |
| Cr layer | Fig. 1 | $161 \pm 5.0$ | $450 \pm 10$ | $7.2 \pm 0.2$ |
| $Al_2O_3$ substrate | $500 \times 10^3$ | $38 \pm 2.0$ | $760 \pm 50$ | $4.0 \pm 0.1$ |

electron transport across the layer is ballistic and scattering is dominated by interfaces, such that suppression of its intrinsic thermal conductivity is inappropriate. Moreover, its equivalent thermal conductance ($k$/thickness) based on bulk Cu or Cr properties is $> 10\,000$ $\mathrm{MW\,m^{-2}\,K^{-1}}$ ($> 25\times$ our largest measured $G$ values), even for the thickest layers, meaning that this assumption has little influence on the predicted $G$ at the $Al_2O_3$ interface. Additionally, we have assumed an infinite thermal interface conductance between the Au layer and the adhesion layer. Typical metal-metal thermal interface conductances are an order of magnitude larger than metal-dielectric interfaces (e.g., $\sim 3.5$ $\mathrm{GW\,m^{-2}\,K^{-1}}$ for the Au/Cu interface [36]), making us insensitive to this value even if it varies with adhesion-layer thickness. Each of the above assumptions may introduce small systematic shifts in the reported $G$, but their influence on the thickness-dependent trends is negligible and not reflected in the uncertainty discussed below. Finally, we choose to report the composite $G$ rather than separating the $G_{e\text{-}p}$ and $G_p$ components in what follows, since the electron-phonon coupling coefficient may be influenced by adhesion-layer thickness. Based on the analysis in Ref. [15], with the reported properties of Cu and Cr [37–41], we estimate electron-phonon coupling conductances of 700 $\mathrm{MW\,m^{-2}\,K^{-1}}$ and 3000 $\mathrm{MW\,m^{-2}\,K^{-1}}$.

The uncertainty in $G$, reported as error bars in Fig. 2, results from the propagation of the uncertainty in the input parameters through the fitting analysis [28]. The major sources of uncertainty are laser spot radius and $Al_2O_3$ thermal conductivity. The $1/e^2$ laser spot radius of $2.8 \pm 0.1$ $\mu$m is measured using the knife-edge technique. $Al_2O_3$ thermal conductivity of $38 \pm 2$ $\mathrm{W\,m^{-1}\,K^{-1}}$ is used for all samples [12]. We quote an uncertainly in our sapphire conductivity in order to reflect the range of reported values in the literature, but the same number (38 $\mathrm{W\,m^{-1}\,K^{-1}}$) is used in all of the analysis and this uncertainty does not affect our conclusions. For the spot size and range of frequencies used in this study, nondiffusive effects are not expected in $Al_2O_3$ because 95% of its thermal conductivity results from phonons with mean free paths less than 1000 nm [42].

## III. RESULTS AND DISCUSSION

The thicknesses of Cu and Cr adhesion layers measured by XRR on the $Al_2O_3$ substrate are shown in Fig. 1. The XRR measurements determined the Au layers to be $71 \pm 2$-nm thick and $70 \pm 2$-nm thick with maximum adhesion-layer thicknesses of $7.3 \pm 0.3$ nm and $8.2 \pm 0.3$ nm at the Cu and Cr wedge edges. One of the XRR fits at an intermediate position on the Cu wedge is shown in the inset of Fig. 1. Positions on the substrate are measured in terms of the normal distance from the flat edge on the $Al_2O_3$ substrates. Nonlinearity in the thickness gradients result from variation in the deposition rate across the target shutter opening. A third-order polynomial fit ($R^2 > 0.99$) to the measured data is used to extract the adhesion-layer thicknesses as a function of position on the substrate.

The thermal interface conductance of Cu and Cr samples is shown in Figs. 2(a) and 2(b) and exhibits an increasing trend as the layers become thicker. In the "nonwedge" region, where only the $Au/Al_2O_3$ interface is present, average $G$ values of $70 \pm 10$ $\mathrm{MW\,m^{-2}\,K^{-1}}$ and $60 \pm 10$ $\mathrm{MW\,m^{-2}\,K^{-1}}$ for Cu and Cr samples are measured.

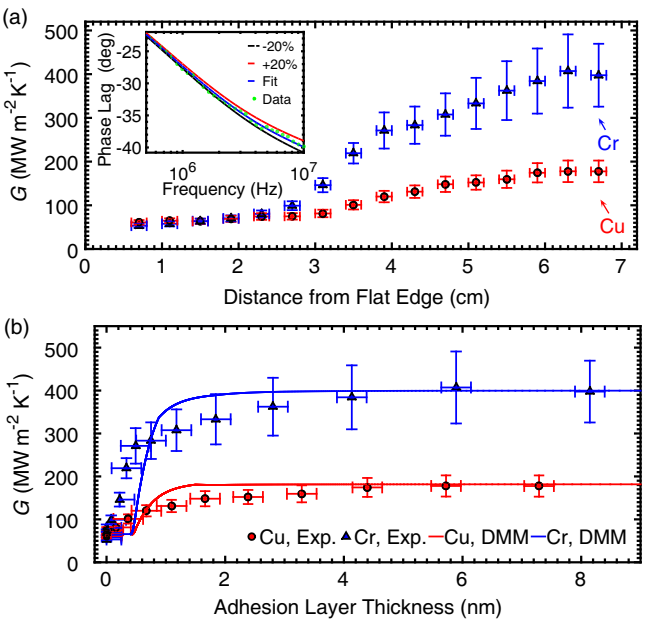


FIG. 2. (a) Experimentally obtained $G$ increases with increasing adhesion-layer thickness for both Cu and Cr. The Cr adhesion layer exhibits a greater increase in $G$ than the Cu with both samples saturating beyond approximately 5 nm. The inset shows the sensitivity of fitting phase-lag data to $\pm 20\%$ of $G$ for the Cr sample at a thickness of 1.10 nm. (b) The experimental values are compared with DMM-based predictions of the accumulation functions of $G$ in terms of Cu or Cr thickness.

This range agrees well with measurements of a $Au/Al_2O_3$ interface reported by Stoner and Maris [10]. Furthermore, as presented in Fig. 2(b), we observe more than twofold and fourfold enhancements of $G$ for 1-nm Cu and Cr adhesion layers, respectively, between the Au and $Al_2O_3$. The measured $G$ saturate at $180 \pm 20\ \mathrm{MW\,m^{-2}\,K^{-1}}$ and $390 \pm 70\ \mathrm{MW\,m^{-2}\,K^{-1}}$, for Cu and Cr adhesion layers, once the layer thickness reached approximately 5 nm. Such a significant enhancement cannot be attributed to an increase in $G_{e\text{-}p}$ in Cu and Cr relative to Au, since this alone would result in a maximum increase of ~20% in $G$, assuming $G_{e\text{-}p}/G_p \cong 5$ in Au. This clearly shows that only a few angstroms of the adhesion layer are needed to significantly increase $G$. From a technological standpoint, this is an important finding for HAMR and other plasmonic devices because thinner adhesion layers will minimize degradation of the optical performance at the plasmonic interface.

To better understand the enhancement in $G$, we compare our measurements with predictions of $G_p$ based on the DMM [42,43]. The DMM is more appropriate than the acoustic mismatch model (AMM) at high temperatures, and as we quantify later, the AMM severely overestimates our experimental data for the $Au/Al_2O_3$ interface [8,44]. A general expression for $G_p$ is [45]

$$G_p = \frac{1}{8\pi^2}\sum_j \int_{K_{j,1}} \hbar\omega_{j,1}(K_{j,1}) K_{j,1}^2 \zeta^{1\to 2} |v_{j,1}(K_{j,1})| \frac{\partial n_0}{\partial T} dK_{j,1}, \tag{1}$$

where 1 signifies material 1 (in this case the metal), $j$ is phonon polarization, $\hbar$ is the reduced Plank constant, $\omega$ is phonon frequency, $K$ is phonon wave vector, $\zeta^{1\to 2}$ is the transmission coefficient of phonons crossing from material 1 to 2, $v$ is phonon group velocity, $n_0$ is the Bose-Einstein distribution of phonons, and $T$ is temperature. This equation can be rewritten as an integral over $\omega$ by substituting $d\omega_{j,1}/dK_{j,1}$ for $v_{j,1}(K_{j,1})$ and canceling $dK_{j,1}$ as follows:

$$\begin{aligned} G_p &= \frac{1}{8\pi^2}\sum_j \int_{\omega_{j,1}} \hbar\omega_{j,1} K_{j,1}^2 \zeta^{1\to 2} \frac{\partial n_0}{\partial T} d\omega_{j,1} \\ &= \sum_j \int_{\omega_{j,1}} g_{j,1}(\omega) d\omega_{j,1}, \end{aligned} \tag{2}$$

where $g_{j,1}$ is a spectral thermal interface conductance per unit $\omega$.

The $\zeta^{1\to 2}$ in Eqs. (1) and (2) needs to be defined for the complete calculation of $G_p$. The DMM assumes diffuse elastic scattering at the interface for all incident phonons as an accepted approach to estimate $\zeta^{1\to 2}$. Notably, the DMM ignores details of the interface and bases its prediction of $\zeta^{1\to 2}$ entirely on the bulk phonon properties in materials 1 and 2. The elastic scattering assumption and detailed balance lead to an expression for $\zeta^{1\to 2}$ as follows [46]:

$$\zeta^{1\to 2}(\omega) = \frac{\sum_j [K_{j,2}(\omega)]^2}{\sum_j [K_{j,1}(\omega)]^2 + \sum_j [K_{j,2}(\omega)]^2}. \tag{3}$$

It is well known that the use of Debye dispersion overestimates contributions of Brillouin-zone edge phonons to $G_p$. Therefore, we instead used real dispersion relationships to calculate $\zeta^{1\to 2}$ and $G_p$ [45,47]. Dispersion relationships for our materials (Au, Cu, Cr, and $Al_2O_3$) are formulated by fitting a fourth-order polynomial to experimentally obtained $\omega$ values as a function of $K$ for each acoustic polarization branch [26,48–51]. The phonon propagation directions in the real dispersion relationships of our materials are chosen to be $\Gamma$-$L$ [111] in Cu and Au, $\Gamma$-$N$ [110] in Cr, and $\Gamma$-$Z$ [0001] for $Al_2O_3$. These directions are chosen based on the $Al_2O_3$ substrate normal direction and on the expected growth texture in each of the films, which differ because Cr is body-centered cubic, while Au and Cu are face-centered cubic [52–56].

To predict $G_p$ as a function of adhesion-layer thickness we assume that only phonons of wavelength ($\lambda$) less than the adhesion-layer thickness ($t$) can exist in the layers. Notably, this assumption disregards changes to the phonon dispersion that may exist in very thin adhesion layers. The assumption that $\lambda_{\max}$ equals $t$ leads us to consider the accumulation of $G_p$ with $\lambda$. A recent study by Cheaito *et al.* [57] described the thermal-interface-conductance accumulation function as a function of $\omega$ as follows:

$$G_{p,\mathrm{accum}}^{1\to 2}(\omega_\alpha) = \sum_j \int_0^{\omega_\alpha} g_{j,1}(\omega) d\omega_{j,1}. \tag{4}$$

The $g_{j,1}(\omega)$ can be converted to $g_{j,1}(\lambda)$ through a change of variables as follows:

$$\begin{aligned} G_{p,\mathrm{accum}}^{1\to 2}(\lambda_\alpha) &= \sum_j \int_{\lambda_{\min}}^{\lambda_\alpha} -g_{j,1}(\omega) \frac{d\omega_{j,1}}{d\lambda_{j,1}} d\lambda_{j,1} \\ &= \sum_j \int_{\lambda_{\min}}^{\lambda_\alpha} g_{j,1}(\lambda) d\lambda_{j,1}, \end{aligned} \tag{5}$$

where $\lambda_{\min}$ is the shortest phonon wavelength defined by $K_{\max}$ at the Brillouin-zone edge. The term $d\omega/d\lambda$ can be analytically evaluated using the relationship between $\omega$ and $K$ that is established in the dispersion relationships and the definition of $K = (2\pi/\lambda)$. Figure 3 shows $g_{j,1}(\lambda)$ for each polarization branch in our metals. The contributions from short $\lambda$ are the largest because the phonon density of states is highest for short $\lambda$—an effect that overpowers their lower relative $v_{j,1}(K_{j,1})$. Discontinuities in $g_{j,1}(\lambda)$ shown in Fig. 3 result from discontinuities in $\zeta^{1\to 2}$ caused by the differing frequency ranges spanned by each polarization (e.g., the transmission of longitudinal modes is higher for frequencies above that spanned by the transverse modes because there are fewer options for reflection).

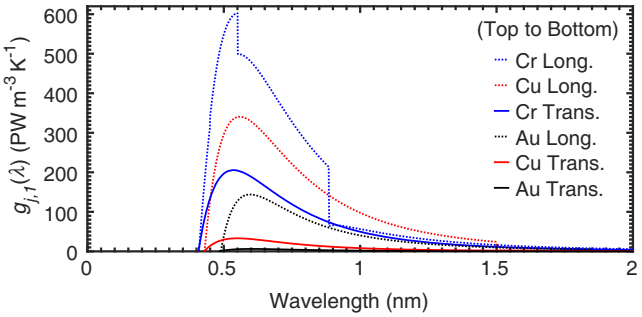


FIG. 3. The interface thermal conductance per unit wavelength, $g_{j,1}(\lambda)$, for each polarization branch in our metallic materials calculated using Eq. (5).

We further assume that phonons with $\lambda$ greater than the adhesion-layer thickness come from the Au layer directly. The physical interpretation of this assumption is that phonons with wavelengths longer than the adhesion layer transmit through it, as if it were transparent. While this assumption is not rigorous, there are many complications to creating a more rigorous model. In particular, the diversity of bonding due to the juxtaposition of three materials would influence the local vibrational states in a nontrivial way. Our approach is a first-order approximation that sheds light on the experimental result and even agrees reasonably, yet has clear shortcomings that are beyond the scope of this study. Therefore, $G(t)$ can be expressed as

$$G_p(t) = G_{p,\mathrm{accum}}^{\mathrm{AL}\rightarrow\mathrm{Al_2O_3}}(t) + [G_{p,\mathrm{Au}\rightarrow\mathrm{Al_2O_3}} - G_{p,\mathrm{accum}}^{\mathrm{Au}\rightarrow\mathrm{Al_2O_3}}(t)], \tag{6}$$

where $G_{p,\mathrm{accum}}^{\mathrm{AL}\rightarrow\mathrm{Al_2O_3}}$ is the accumulated $G_p$ as a function of adhesion-layer (AL) thickness, $G_{p,\mathrm{Au}\rightarrow\mathrm{Al_2O_3}}$ is the maximum value of $G_{p,\mathrm{accum}}^{\mathrm{Au}\rightarrow\mathrm{Al_2O_3}}(t)$, and $G_p(t)$ is the accumulated $G_p$ as a function of the adhesion-layer thickness.

The calculated $G_p(t)$ at 300 K is plotted in Fig. 2(b). A plateau in the predicted $G_p(t)$ occurs for adhesion-layer thicknesses greater than ~2 nm. The maximum predicted values are 180 MW m$^{-2}$ K$^{-1}$ and 400 MW m$^{-2}$ K$^{-1}$, which are in reasonable agreement with our measured values of the thickest Cu and Cr films. The AMM, on the other hand, highly overestimates our results, yielding ~300 MW m$^{-2}$ K$^{-1}$, ~540 MW m$^{-2}$ K$^{-1}$, and ~900 MW m$^{-2}$ K$^{-1}$ for $Al_2O_3$ interfaces with Au, Cu, and Cr. Notably, the predictions of $G_p$ exclude $G_{e\text{-}p}$, while it is included in the measured $G$ as previously discussed. The fact that the DMM captures our observed accumulation with thickness suggests that it may be a reasonable predictive tool—even for very thin adhesion layers. An alternative DMM interpretation may be that $\lambda_{\max} = 2t$, which would cause faster accumulation with thickness. Given the uncertainty of our thickness measurement, we cannot use this data set to confirm whether adhesive effects at the interface play a significant role for thicknesses less than the minimum phonon wavelength [25]. Excluding this range, the difference between the DMM and experiment is not great enough to require the invocation of additional interfacial mechanisms at work in determining phonon transmission, beyond alignment of the density of states of the two interfaced materials.

## IV. CONCLUSIONS

We measure a significant increase in $G$ at the metal-dielectric $Au/Al_2O_3$ interface as a function of Cu and Cr adhesion-layer thickness inserted between Au and $Al_2O_3$. Both Cu and Cr show a saturation of $G$ ($390 \pm 70$ MW m$^{-2}$ K$^{-1}$ in Cr and $180 \pm 20$ MW m$^{-2}$ K$^{-1}$ in Cu) once the layer thickness exceeds 5 nm. From a plasmonic technological perspective, having a very thin adhesion layer minimizes disruption of the optical properties that are critical to plasmonic performance. The experimentally observed $G$ values are compared with predictions, where the transmission coefficients are obtained using the DMM with real dispersion relationships. Calculated and experimental values agree, suggesting that phonon alignment is indeed a dominant mechanism in increasing $G$ with very thin adhesion layers, rather than the enhancement of electron-phonon coupling on the metal side of the interface. Notably, the use of a metal adhesion layer at the metal-dielectric interface also generates a new metal-metal interface that is not herein a focal point. Because electrons transmit efficiently between metal layers, this metal-metal interface has very high thermal conductance, and therein plays a small role in the total $G$. Dielectric adhesion layers would instead introduce two phonon-dominated interfaces, though they could still be beneficial for adhesion and bridging of dissimilar phonon states.

## ACKNOWLEDGMENTS

We acknowledge financial support from the National Science Foundation (NSF CBET 1403447) and the Data Storage Systems Center (DSSC) at Carnegie Mellon University, as well as helpful discussions with John C. Duda from Seagate Technology.

[1] C. L. Kane and E. J. Mele, Quantum Spin Hall Effect in Graphene, Phys. Rev. Lett. **95**, 226801 (2005).
[2] Haijun Zhang, Chao-Xing Liu, Xiao-Liang Qi, Xi Dai, Zhong Fang, and Shou-Cheng Zhang, Topological insulators in $Bi_2Se_3$, $Bi_2Te_3$ and $Sb_2Te_3$ with a single Dirac cone on the surface, Nat. Phys. **5**, 438 (2009).
[3] M. Z. Hasan and C. L. Kane, Colloquium: Topological insulators, Rev. Mod. Phys. **82**, 3045 (2010).
[4] Vincent Sacksteder, Tomi Ohtsuki, and Koji Kobayashi, Modification and Control of Topological Insulator Surface

States Using Surface Disorder, Phys. Rev. Applied **3**, 064006 (2015).

[5] W. A. Challener, Chubing Peng, A. V. Itagi, D. Karns, Wei Peng, Yingguo Peng, XiaoMin Yang, Xiaobin Zhu, N. J. Gokemeijer, Y.-T. Hsia, G. Ju, Robert E. Rottmayer, Michael A. Seigler, and E. C. Gage, Heat-assisted magnetic recording by a near-field transducer with efficient optical energy transfer, Nat. Photonics **3**, 220 (2009).

[6] Zhi-Min Yuan, Jianzhong Shi, Chun Lian Ong, P. S. Alexopoulos, Chunling Du, Anmin Kong, Shiming Ang, B. Santoso, Siang Huei Leong, Kheong Sann Chan, Yibin Ng, Kui Cai, J. Tsai, Hanxiang Ng, and Hang Khume Tan, Dedicated servo recording system and performance evaluation, IEEE Trans. Magn. **51**, 1 (2015).

[7] L. Huang, B. Stipe, M. Staffaroni, J.-Y. Juang, T. Hirano, E. Schreck, and F.-Y. Huang, HAMR thermal modeling including media hot spot, IEEE Trans. Magn. **49**, 2565 (2013).

[8] E. T. Swartz and R. O. Pohl, Thermal boundary resistance, Rev. Mod. Phys. **61**, 605 (1989).

[9] Yibin Xu, Haitao Wang, Yoshihisa Tanaka, Masato Shimono, and Masayoshi Yamazaki, Measurement of interfacial thermal resistance by periodic heating and a thermoreflectance technique, Mater. Trans., JIM **48**, 148 (2007).

[10] R. J. Stoner and H. J. Maris, Kapitza conductance and heat flow between solids at temperatures from 50 to 300 K, Phys. Rev. B **48**, 16373 (1993).

[11] Robert J. Stevens, Andrew N. Smith, and Pamela M. Norris, Measurement of thermal boundary conductance of a series of metal-dielectric interfaces by the transient thermoreflectance technique, J. Heat Transfer **127**, 315 (2005).

[12] Kimberlee C. Collins, Alexei A. Maznev, John Cuffe, Keith A. Nelson, and Gang Chen, Examining thermal transport through a frequency-domain representation of time-domain thermoreflectance data, Rev. Sci. Instrum. **85**, 124903 (2014).

[13] J. Lombard, F. Detcheverry, and S. Merabia, Influence of the electron-phonon interfacial conductance on the thermal transport at metal/dielectric interfaces, J. Phys. Condens. Matter **27**, 015007 (2015).

[14] Yan Wang, Xiulin Ruan, and Ajit K. Roy, Two-temperature nonequilibrium molecular dynamics simulation of thermal transport across metal-nonmetal interfaces, Phys. Rev. B **85**, 205311 (2012).

[15] Arun Majumdar and Pramod Reddy, Role of electron-phonon coupling in thermal conductance of metal-nonmetal interfaces, Appl. Phys. Lett. **84**, 4768 (2004).

[16] R. E. Jones, J. C. Duda, X. W. Zhou, C. J. Kimmer, and P. E. Hopkins, Investigation of size and electronic effects on Kapitza conductance with non-equilibrium molecular dynamics, Appl. Phys. Lett. **102**, 183119 (2013).

[17] Patrick E. Hopkins, John C. Duda, Bryan Kaehr, Xiao Wang Zhou, C.-Y. Peter Yang, and Reese E. Jones, Ultrafast and steady-state laser heating effects on electron relaxation and phonon coupling mechanisms in thin gold films, Appl. Phys. Lett. **103**, 211910 (2013).

[18] Piyush Singh, Myunghoon Seong, and Sanjiv Sinha, Detailed consideration of the electron-phonon thermal conductance at metal-dielectric interfaces, Appl. Phys. Lett. **102**, 181906 (2013).

[19] R. B. Wilson, Joseph P. Feser, Gregory T. Hohensee, and David G. Cahill, Two-channel model for nonequilibrium thermal transport in pump-probe experiments, Phys. Rev. B **88**, 144305 (2013).

[20] Edward Dechaumphai, Dylan Lu, Jimmy J. Kan, Jaeyun Moon, Eric E. Fullerton, Zhaowei Liu, and Renkun Chen, Ultralow thermal conductivity of multilayers with highly dissimilar Debye temperatures, Nano Lett. **14**, 2448 (2014).

[21] A. V. Sergeev, Electronic Kapitza conductance due to inelastic electron-boundary scattering, Phys. Rev. B **58**, R10199 (1998).

[22] Wei Wang and David G. Cahill, Limits to Thermal Transport in Nanoscale Metal Bilayers due to Weak Electron-Phonon Coupling in Au and Cu, Phys. Rev. Lett. **109**, 175503 (2012).

[23] I. M. Lifshits and M. I. Kaganov, Relaxation between electrons and crystalline lattice, Zh. Eksp. Teor. Fiz. **31**, 232 (1957) Sov. Phys. JETP **4**, 173 (1957)].

[24] J. C. Duda, C.-Y. P. Yang, B. M. Foley, R. Cheaito, D. L. Medlin, R. E. Jones, and P. E. Hopkins, Influence of interfacial properties on thermal transport at gold:silicon contacts, Appl. Phys. Lett. **102**, 081902 (2013).

[25] Timothy S. English, John C. Duda, Justin L. Smoyer, Donald A. Jordan, Pamela M. Norris, and Leonid V. Zhigilei, Enhancing and tuning phonon transport at vibrationally mismatched solid-solid interfaces, Phys. Rev. B **85**, 035438 (2012).

[26] See Supplemental Material at http://link.aps.org/supplemental/10.1103/PhysRevApplied.5.014009 for surface characteristics of our grown films, uncertainties in the x-ray reflectivity (XRR) measurements of thickness, and our formulated dispersion relationships.

[27] Wee-Liat Ong, Sara M. Rupich, Dmitri V. Talapin, Alan J. H. McGaughey, and Jonathan A. Malen, Surface chemistry mediates thermal transport in three-dimensional nanocrystal arrays, Nat. Mater. **12**, 410 (2013).

[28] Jonathan A. Malen, Kanhayalal Baheti, Tao Tong, Yang Zhao, Janice A. Hudgings, and Arun Majumdar, Optical measurement of thermal conductivity using fiber aligned frequency domain thermoreflectance, J. Heat Transfer **133**, 081601 (2011).

[29] Aaron J. Schmidt, Xiaoyuan Chen, and Gang Chen, Pulse accumulation, radial heat conduction, and anisotropic thermal conductivity in pump-probe transient thermoreflectance, Rev. Sci. Instrum. **79**, 114902 (2008).

[30] David G. Cahill, Analysis of heat flow in layered structures for time-domain thermoreflectance, Rev. Sci. Instrum. **75**, 5119 (2004).

[31] A. Göbel, F. Hemberger, S. Vidi, and H.-P. Ebert, A new method for the determination of the specific heat capacity using laser-flash calorimetry down to 77 K, Int. J. Thermophys. **34**, 883 (2013).

[32] R. H. Beaumont, H. Chihara, and J. A. Morrison, An anomaly in the heat capacity of chromium at $38 \cdot 5\,^{\circ}\mathrm{C}$, Philos. Mag. **5**, 188 (1960).

[33] Fran Cverna *et al.*, *ASM Ready Reference: Thermal Properties of Metals* (ASM International, Materials Park, 2002).

[34] Keith T. Regner, Daniel P. Sellan, Zonghui Su, Cristina H. Amon, Alan J. H. McGaughey, and Jonathan A. Malen, Broadband phonon mean free path contributions to thermal

conductivity measured using frequency domain thermoreflectance, Nat. Commun. **4**, 1640 (2013).
[35] Mark D. Losego, Martha E. Grady, Nancy R. Sottos, David G. Cahill, and Paul V. Braun, Effects of chemical bonding on heat transport across interfaces, Nat. Mater. **11**, 502 (2012).
[36] Bryan C. Gundrum, David G. Cahill, and Robert S. Averback, Thermal conductance of metal-metal interfaces, Phys. Rev. B **72**, 245426 (2005).
[37] J. P. Moore, R. K. Williams, and R. S. Graves, Thermal conductivity, electrical resistivity, and Seebeck coefficient of high-purity chromium from 280 to 1000 K, J. Appl. Phys. **48**, 610 (1977).
[38] S. D. Brorson, A. Kazeroonian, J. S. Moodera, D. W. Face, T. K. Cheng, E. P. Ippen, M. S. Dresselhaus, and G. Dresselhaus, Femtosecond Room-Temperature Measurement of the Electron-Phonon Coupling Constant $\gamma$ in Metallic Superconductors, Phys. Rev. Lett. **64**, 2172 (1990).
[39] H. E. Elsayed-Ali, T. B. Norris, M. A. Pessot, and G. A. Mourou, Time-Resolved Observation of Electron-Phonon Relaxation in Copper, Phys. Rev. Lett. **58**, 1212 (1987).
[40] R. E. B. Makinson, The thermal conductivity of metals, Math. Proc. Cambridge Philos. Soc. **34**, 474 (1938).
[41] Alexander A Balandin, Thermal properties of graphene and nanostructured carbon materials, Nat. Mater. **10**, 569 (2011).
[42] Yongjie Hu, Lingping Zeng, Austin J Minnich, Mildred S Dresselhaus, and Gang Chen, Spectral mapping of thermal conductivity through nanoscale ballistic transport, Nat. Nanotechnol. **10**, 701 (2015).
[43] Robert J. Stevens, Pamela M. Norris, and Leonid V. Zhigilei, Molecular dynamics study of thermal boundary resistance: Evidence of strong inelastic scattering transport channels, in *Proceedings of the ASME 2004 International Mechanical Engineering Congress and Exposition, Anaheim, 2004* (ASME, New York, 2004), pp. 37–46.
[44] M. Kazan, Interpolation between the acoustic mismatch model and the diffuse mismatch model for the interface thermal conductance: Application to InN/GaN superlattice, J. Heat Transfer **133**, 112401 (2011).
[45] John C. Duda, Thomas E. Beechem, Justin L. Smoyer, Pamela M. Norris, and Patrick E. Hopkins, Role of dispersion on phononic thermal boundary conductance, J. Appl. Phys. **108**, 073515 (2010).
[46] John C. Duda, Justin L. Smoyer, Pamela M. Norris, and Patrick E. Hopkins, Extension of the diffuse mismatch model for thermal boundary conductance between isotropic and anisotropic materials, Appl. Phys. Lett. **95**, 031912 (2009).
[47] Pramod Reddy, Kenneth Castelino, and Arun Majumdar, Diffuse mismatch model of thermal boundary conductance using exact phonon dispersion, Appl. Phys. Lett. **87**, 211908 (2005).
[48] J. W. Lynn, H. G. Smith, and R. M. Nicklow, Lattice dynamics of gold, Phys. Rev. B **8**, 3493 (1973).
[49] H. Schober, D. Strauch, and B. Dorner, Lattice dynamics of sapphire ($Al_2O_3$), Z. Phys. B **92**, 273 (1993).
[50] Ruqing Xu, Hawoong Hong, Paul Zschack, and T.-C. Chiang, Direct Mapping of Phonon Dispersion Relations in Copper by Momentum-Resolved X-Ray Calorimetry, Phys. Rev. Lett. **101**, 085504 (2008).
[51] L. D. Muhlestein and W. M. Shaw, Investigation of the phonon dispersion relations of chromium by inelastic neutron scattering, Phys. Rev. B **4**, 969 (1971).
[52] Takeo Sasaki, Katsuyuki Matsunaga, Hiromichi Ohta, Hideo Hosono, Takahisa Yamamoto, and Yuichi Ikuhara, Atomic and electronic structures of $Cu/\alpha$-$Al_2O_3$ interfaces prepared by pulsed-laser deposition, Sci. Technol. Adv. Mater. **4**, 575 (2003).
[53] Zoe Boekelheide and F Hellman, Cr (110) texture induced by epitaxy on $Al_2O_3$ (0001) substrates: Preferential grain growth in the $\langle 001 \rangle$ direction, Appl. Phys. Lett. **102**, 141601 (2013).
[54] S Tsukimoto, F Phillipp, and T Wagner, Texture of MBE grown Cr films on $\alpha$-$Al_2O_3$ (0001): The occurrence of Nishiyama-Wassermann (NW) and Kurdjumov-Sachs (KS) related orientation relationships, J. Eur. Ceram. Soc. **23**, 2947 (2003).
[55] Christine Marie Montesa, Naoya Shibata, Tetsuya Tohei, Kazuhiro Akiyama, Yoshirou Kuromitsu, and Yuichi Ikuhara, Application of coincidence of reciprocal lattice point model to metal/sapphire hetero interfaces, Mater. Sci. Eng. B **173**, 234 (2010).
[56] Hila Sadan and Wayne D Kaplan, Au–sapphire (0001) solid–solid interfacial energy, J. Mater. Sci. **41**, 5099 (2006).
[57] Ramez Cheaito, John T. Gaskins, Matthew E. Caplan, Brian F. Donovan, Brian M. Foley, Ashutosh Giri, John C. Duda, Chester J. Szwejkowski, Costel Constantin, Harlan J. Brown-Shaklee, Jon F. Ihlefeld, and Patrick E. Hopkins, Thermal boundary conductance accumulation and interfacial phonon transmission: Measurements and theory, Phys. Rev. B **91**, 035432 (2015).